

www.acsanm.org Article

Overcoming Losses through Phase Locking in Nonlinear Quasi-Bound States in the Continuum Metasurfaces

Jiannan Gao, Maria Antonietta Vincenti, Jesse A. Frantz, Anthony Clabeau, Xingdu Qiao, Liang Feng, Michael Scalora, and Natalia Litchinitser*



Cite This: ACS Appl. Nano Mater. 2024, 7, 21445-21452



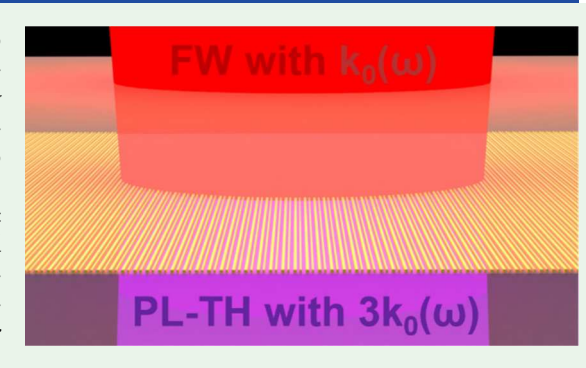
ACCESS I

III Metrics & More

Article Recommendations

SI Supporting Information

ABSTRACT: The development of nonlinear flat-optic nanostructures, also known as optical metasurfaces, offers unprecedented enhancement of light-matter interactions without the need for phase matching, potentially revolutionizing future applications in integrated nonlinear optics. Quasi-bound states in the continuum (qBIC) have demonstrated the ability to achieve high-quality resonances with substantial field enhancement. However, most prior studies were limited to the first-order magnetic dipole qBIC resonances, where the enhanced electric field is concentrated in the regions outside rather than inside the high refractive index metaatoms. In contrast, concentrating the electric field primarily within the high-index nonlinear resonators could significantly boost nonlinear light-matter interactions and enhance the conversion efficiency. Here, we demonstrate a



qBIC-resonance-based metasurface designed to localize the electric field inside the high-index nonlinear meta-atoms and enhance conversion efficiency. The demonstrated high conversion efficiency is achieved even within the material's highly absorbing spectral range due to phase locking.

KEYWORDS: Bound state in the continuum, nonlinear metasurface, chalcogenide, phase-locking, all-optical tunability

1. INTRODUCTION

Photonic bound states in the continuum (BICs), which are nonradiating states of light embedded within the continuum of propagating modes, have recently attracted much attention because of the extreme localization and substantial enhancement of the electromagnetic field at the nanoscale. 1-4 BIC states are crucial for many applications, including topological photonics, quantum, and nonlinear optics. 5-13 Ideal symmetryprotected BICs, possessing infinite lifetimes and quality factors, exist as bound eigenmodes above the photonic light line and do not radiate into the far field. While ideal BICs are entirely decoupled from the radiation continuum and therefore cannot be excited in realistic settings, in practice, they can be turned into a leaky Fano line-shape resonance, also known as a quasi-BIC (qBIC) resonance, by slightly perturbing the structure geometry or the conditions of the surrounding environment. 14-17 Recent studies have demonstrated that dielectric metasurfaces with in-plane asymmetry can induce destructive interference between leaky modes, creating a qBIC state with controllable radiative losses that are proportional to the square of the asymmetry parameter. 15,18,19 The qBIC resonances are widely used in various nanophotonics subwavelength resonators in the visible, infrared, THz, and microwave frequency ranges for sensing, Raman lasing, hologram, chiral emission, and nonlinear wavelength conversion applications. 20-27

Nonlinear wavelength conversion, such as second harmonic generation (SHG) and third harmonic generation (THG), is essential for extending the spectral range of laser sources to wavelengths that are challenging to reach with conventional laser gain media. Moreover, the demand for compact, highefficiency, and multifunctional devices that can replace traditional bulky, free-space technologies is continuously rising, especially in the ultraviolet (UV) region. Indeed, coherent UV sources are essential for many applications, including cell sorting, sensing, data storage, semiconductor processing, as well as military and space technologies.^{28,29} Currently, efficient wavelength conversion in an integrated, compact, tunable UV source is possible only using nonlinear optical materials that are simultaneously transparent in the UV, possess high and fast nonlinear susceptibility, and are at the same time, birefringent. Chalcogenide glasses have emerged as a promising platform for many on-chip applications at mid- and near-infrared wavelengths due to their high linear refractive indices, phase change properties, and strong Kerr nonlinearity. $^{30-36}$ We have notably

Received: June 3, 2024
Revised: August 27, 2024
Accepted: August 29, 2024
Published: September 16, 2024





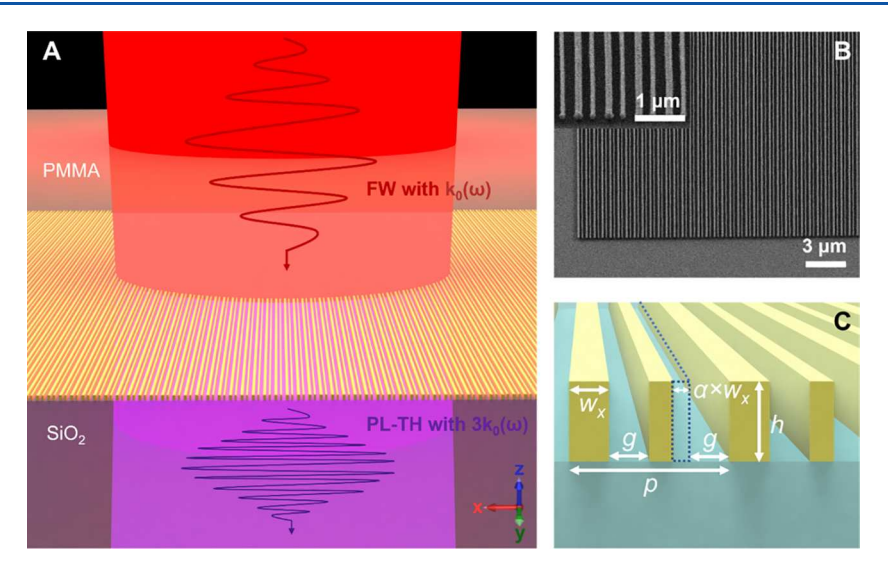


Figure 1. Third harmonic generation in a chalcogenide qBIC metasurface. (A) Arsenic trisulfide (As₂S₃) metasurface on a fused silica substrate with a PMMA layer on top. Patterned As₂S₃ structure of 400 μ m × 400 μ m, consisting of asymmetric pairs of nanowires. (B) The 30° tilted SEM image of the fabricated metasurface sample. The inset image provides a magnified look at the structure. (C) Schematic of the unit cell with broken in-plane symmetry. The p, h, g, w_x, and α are the period and the height of the unit cell, the width of the gap between two nanowires in one unit cell, the width of the nanowire, and the asymmetry parameter, respectively. In our investigation, p = 580 nm, h = 300 nm, g = 145 nm, w_x = 145 nm, and α varies from 0 to 0.4.

demonstrated ultrafast, tunable frequency conversion from near-infrared to ultraviolet in a chalcogenide glass metasurface, using Mie resonances and a phase-locking mechanism between the pump and the inhomogeneous portion of the TH signal.³⁷⁻³⁹ This phase locking allows the pump pulse and the inhomogeneous harmonic component to copropagate, sharing the same refractive index and absorption coefficient as the pump. 40,41 When this process occurs within a cavity, efficient frequency conversion is possible, even in the presence of strong material absorption at the harmonic wavelengths. 42,43 As with all nonlinear processes, a resonant condition at the pump field significantly enhances the nonlinear interactions. However, the conversion efficiency from the low-order magnetic field Mie resonance is essentially limited by its appreciable coupling with the radiative continuum and can be greatly enhanced by using qBIC resonances with significantly higher Q factor and stronger localization and enhancement of the electric field. 18,44,45 However, most prior studies focus on the first-order magnetic dipole qBIC, where the enhanced electric fields are concentrated around the edges rather than in the center of the high refractive index nonlinear material metaatoms. In contrast, localizing the electric field primarily within the high-index nonlinear material could significantly boost nonlinear light-matter interactions and enhance the conversion efficiency. This work shows how different qBIC modes can affect nonlinear processes differently. We theoretically predict and experimentally demonstrate strongly boosted and tunable THG in the UV wavelength region from a judiciously designed As₂S₃-based metasurface where an electric dipole (ED)-qBIC resonance is excited near 1070 nm. We can benefit from an exceptional field enhancement at the pump frequency from the excitation of quasi-bound states in the continuum that boosts the phase-locked third harmonic component. Combining these two conditions allows for exploiting nonlinear interactions, even in the high absorption region of the material.

2. EXPERIMENTAL SECTION

Let us begin by examining the transmission of a pump pulse across the boundary between a linear medium and a nonlinear medium. In the absence of phase matching, three harmonic components are generated: one is reflected back into the linear medium, while the other two are transmitted. When phase matching conditions are met, however, the two transmitted components merge into a single degenerate component. References^{40,42} have provided a detailed theoretical description of this process, which includes homogeneous and inhomogeneous components based on the solution of Maxwell's equations. In the absence of absorption, the homogeneous TH component propagates with a group velocity that corresponds to the material dispersion at the TH wavelength. In contrast, the inhomogeneous TH component, also known as the phase-locked (PL) component 41,43 is captured by the pump pulse and copropagates with a wavenumber given by $k_{\text{INHOM}} = 3k_0(\omega)n(\omega)$. The PL components only form in the presence of an interface or feedback, as demonstrated in previous studies. 41 Although the harmonic fields are captured by the pump and propagate together under anomalous dispersive conditions, energy exchange occurs only at the suboptical cycle time frame if we consider harmonic components of the energy. Therefore, to the first order of approximation, there is no energy exchange between the fundamental frequency (FF) and its PL components in a bulk medium, regardless of material thickness, as verified in experimental studies. 46,4

We will now delve into the design of our metasurfaces, which support q-BIC modes. The schematic of the proposed metasurface device is depicted in Figure 1A. The metasurface consists of As₂S₃ nanowires patterned on a glass substrate, with the poly(methyl methacrylate) (PMMA) spin-coated on top. This configuration ensures that the metasurface is surrounded by materials with similar refractive indices. The fabrication procedure is shown in Supporting Note 1. This configuration results in significantly improved field localization within the As₂S₃ nanowires compared to structures without PMMA (where air is present on top) and also protects the As₂S₃ structure from degradation. Figure 1B shows the scanning electron microscopy (SEM) image of the fabricated As₂S₃ metasurface sample. The geometrical parameters of the metasurface shown in Figure 1B are optimized to enhance third harmonic generation (THG) efficiency in the UV wavelength range using an ED-qBIC resonance near 1070 nm. A set of asymmetric nanowire unit cells with period p = 580 nm and height h = 300 nm are placed on top of a glass

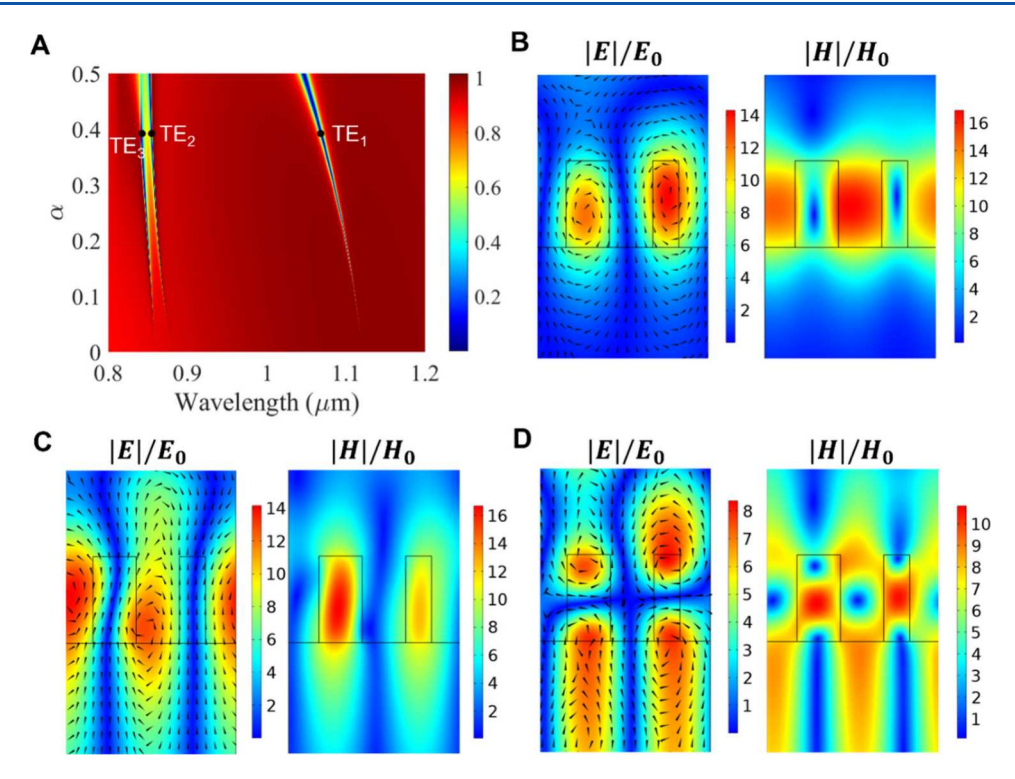


Figure 2. (A) Numerically simulated transmittance as a function of the wavelength and asymmetry factor α . (B) Electric and magnetic field enhancement ratio for $\alpha = 0.4$ at the TE₁ (ED-qBIC) mode located at 1070 nm: (C) Same as in B for the TE₂ (MD-qBIC) mode located at 854 nm; (D) Same as in B and C for the TE₃ (EQ-qBIC) mode located at 841 nm. The black arrows represent the magnetic field.

substrate. Other parameters include the width of the nanowires w_x = 145 nm and the asymmetry parameter of the unit cell α that controls the width of one nanowire. The theoretical investigation considers asymmetry parameter α from 0 to 0.4 (see Figure 1C) so that the width of the narrower element varies from 145 to 87 nm. The asymmetry parameter is the key to transforming the ideal (decoupled) BIC system into the qBIC, supporting high-Q leaky resonant modes. The electric field of the incident beam at the fundamental frequency (FF) is polarized along the y direction. We used a spectroscopic ellipsometer to measure the refractive index of a 300 nm thick As₂S₃ film (see Supporting Note 2) and incorporated the measured data into our design and numerical simulations. The ellipsometry data indicate that As₂S₃ exhibits a strong dispersion and high absorption at wavelengths below 500 nm, which is where the TH wavelength is generated.

The commercial Finite Element Method simulation package Comsol Multiphysics 6.0 was used to perform both linear and nonlinear simulations. The measured refractive index of As₂S₃ from the ellipsometer was used in the simulations. For both the glass substrate and the PMMA superstrate, a constant refractive index of 1.5 was assumed. The simulated linear transmittance represents an average result obtained by varying the incident beam angle between -3 and 3 degrees. Nonlinear simulations were conducted using a fully coupled solver, with values for $\chi^{(3)}(\omega)$ and $\chi^{(3)}(3\omega)$ obtained through the numerical method detailed in ref 48. The third-order nonlinear susceptibility $\chi^{(3)}(\omega)$ at the fundamental frequency (ω) is used to model the refractive index change induced by the intense optical field and the third-order nonlinear susceptibility $\chi^{(3)}(3\omega)$ at the third harmonic frequency (3ω) is used to describe the nonlinear response of the material to the incident optical field at the third harmonic frequency. Nonlinear susceptibility data was treated as a fit parameter to achieve the best agreement between simulations and experimental results.

3. RESULTS AND DISCUSSION

The designed metasurface can support different qBIC modes, providing different field localization profiles and enhance-

ments. Figure 2A shows the simulated transmittances of As₂S₃ metasurfaces with period p = 580 nm and height h = 300 nm and variable asymmetry parameter α in the range of wavelengths from 800 nm to 1100 nm, assuming normal incidence. Three qBIC modes can be identified in the map. To understand the differences between the modes, we set $\alpha = 0.4$. For this asymmetry factor, we find the lowest-order mode at 1070 nm (point labeled TE₁ in the map). This mode shows high electric field localization in the nanowires and a magnetic field that experiences symmetry breaking, and it is localized in the gap between the nanowires. In other words, this qBIC mode resembles an electric-dipole-like (ED-qBIC) localization (Figure 2B). By using the incident electric field as the baseline, it achieves a maximum electric field amplitude enhancement by a factor of approximately 15. A second qBIC mode appears at lower wavelengths (point labeled TE₂ on the map). This mode is located at 854 nm for $\alpha = 0.4$: Figure 2C shows that this mode resembles a magnetic dipole (MD-qBIC), with a field localization dual with respect to the ED-qBIC, and therefore with an electric field mainly located outside the nanowires. Finally, the third mode (point labeled TE₃ in the map) is located at 841 nm. It possesses an electric-quadrupole-like localization (EQ-qBIC), with the electric field located once again mainly inside the nanowires. We also stress that since the EQ-BIC mode falls near the onset of the first diffraction order of the periodic structure, we observe a hybridization between a leaky (guided mode resonance) and a quasi-bound mode (Figure 2D) rather than a strongly confined mode as for the ED- and MD-qBICs. A detailed band structure analysis of the mode hybridization can be found in Supporting Note 3. Since the ED-qBIC provides an electric field mainly concentrated in the high-index nonlinear material, we can predict that this mode would be the most appropriate to improve nonlinear

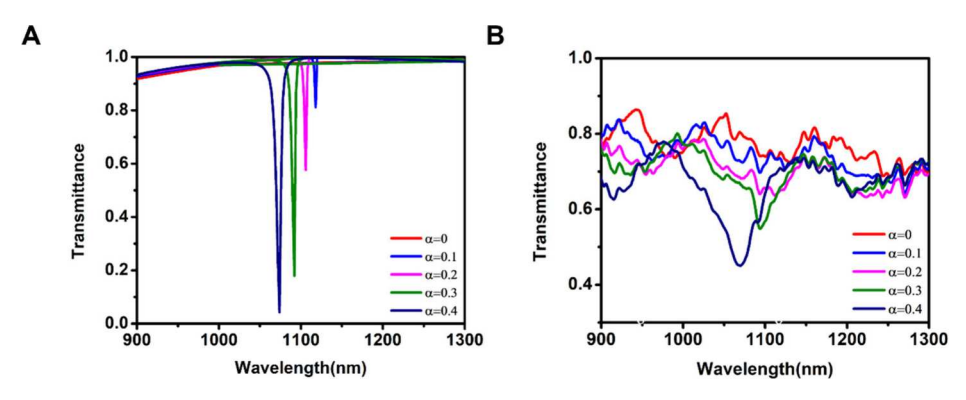


Figure 3. Transmission from the chalcogenide ED-qBIC metasurfaces. (A) The simulated and (B) measured transmittances of the designed sample agree.

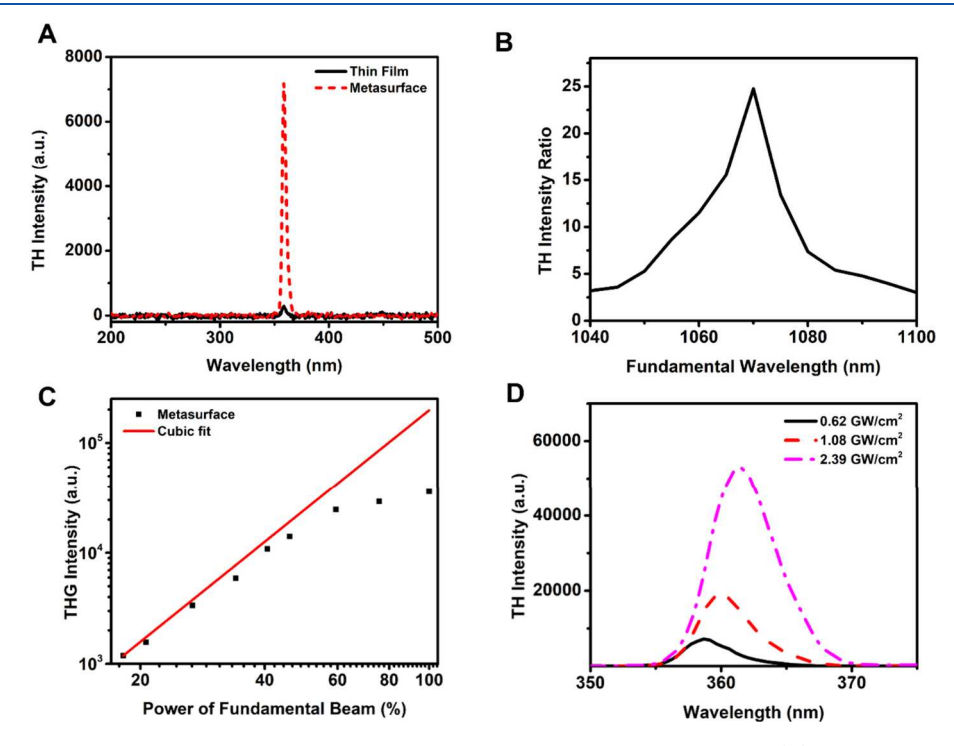


Figure 4. Third harmonic generation from the chalcogenide metasurface at the ED-qBIC resonance. (A) TH intensity was measured for the uniform thin film of As_2S_3 covered by PMMA (black, solid curve) compared to the nanowire-based metasurface (red, dashed-dotted curve). B: Experimental results showing THG enhancement for the metasurface relative to the reference sample, with the peak THG intensity from the metasurface being approximately 24 times greater. (C) THG power dependence as a function of the fundamental beam power. (D) Measured shift in THG with increasing intensity of the fundamental beam.

light-matter interactions and to enhance the conversion efficiency of THG (a comparison of the three qBIC modes in terms of third harmonic conversion efficiency is shown in Supporting Note 4).

Moreover, while a mere conversion efficiency estimate could serve as a guideline to experiment if the pulse that excites the metasurface has a relatively wide bandwidth (our nonlinear experiment was performed with a 100 fs long pulse, corresponding to a full-width-at-half-maximum of ~17 nm at 1070 nm), one may conclude that it is beneficial to use wider ED-qBIC resonances rather than a narrower MD-qBIC resonance to optimize the resonant light-matter interaction at the fundamental wavelength.

We, therefore, proceeded to characterize the ED-qBIC transmission dip. Figure 3 compares the simulated (Figure 3A) and measured (Figure 3B) transmittance spectra obtained for different fabricated asymmetry factors. The detailed descrip-

tion of the linear measurement setup was described in the ref.³⁸ We note that the measured ED-qBIC resonance dips are broader and shallower than those obtained in numerical simulations, which can be attributed to several factors: First, the nanofabrication-related inaccuracies in the dimensions and periodicity can affect the results. The fabricated nanostructures have slightly larger periods, widths, and asymmetry factor. Second, imperfect alignment may cause the sample to deviate from the normal angle of incidence, leading to unwanted noise in the transmission measurement. Other experimental conditions, such as light intensity, can also contribute to the noise observed in the transmission data. However, we managed to minimize these noise sources as much as possible to obtain accurate measurements. The theoretical and experimental Qfactors from the sample for the sample with an asymmetry factor of $\alpha = 0.4$ are approximately 178 and 15, respectively. Figure S5 in Supporting Note 5 demonstrates that incorporat-

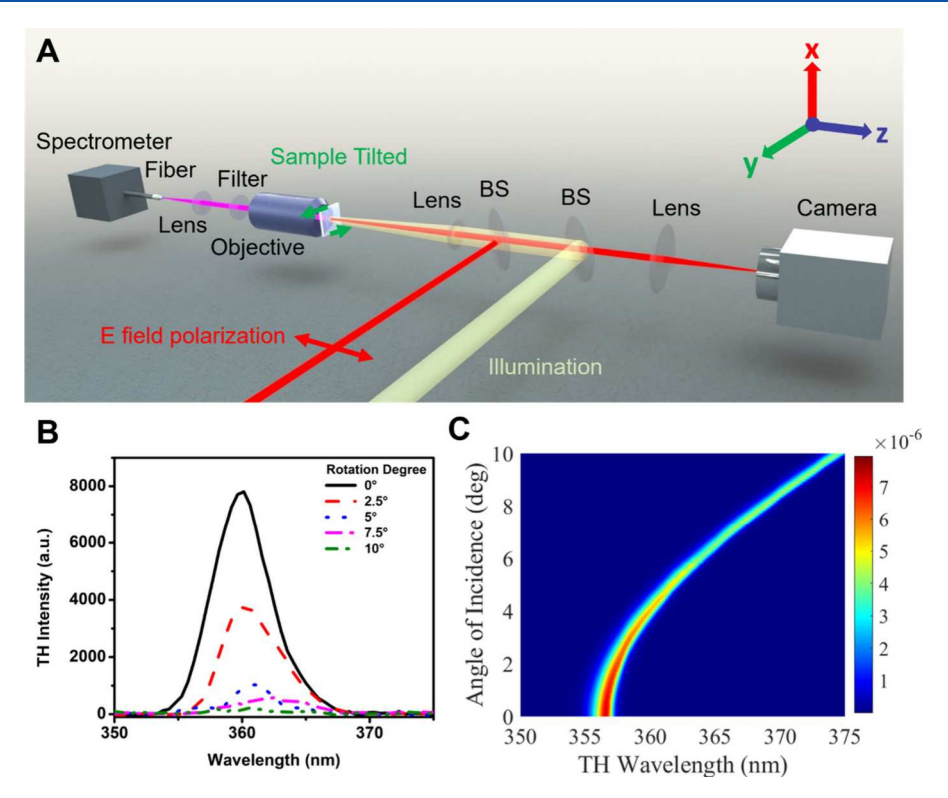


Figure 5. Third harmonic generation with a rotation angle of the metasurfaces. (A) Schematic illustration of the experimental setup. The (B) measured and (C) simulated angular dependences of the TH power and wavelength.

ing nanofabrication imperfections into numerical simulations leads to a broader and shallower resonance with a Q-factor of 12.5. There are several methods to enhance the quality of metasurfaces further. First, fabrication precision can be improved by using industry-grade (as opposed to universitygrade) nanofabrication tools, improving the accuracy and reliability of metasurface manufacturing. Second, the size of the metasurface structures can be increased by reducing the refractive index of the surrounding medium. Lowering the refractive index of the surrounding medium effectively extends the effective wavelength of light, enabling larger physical dimensions for the metasurface elements. This size increase can facilitate easier fabrication, allowing for greater tolerances in alignment and patterning. Despite the presence of noise in our experimental data, our results, standing as a compelling proof-of-concept, unequivocally demonstrate the significance of our research. Moreover, both simulated and measured spectra show excellent agreement with respect to the blue shift of the resonance when the asymmetry is increased. Such a blue shift of the mode is also clearly visible in the map in Figure 2A.

We then performed nonlinear characterization of the sample. We investigated the enhanced THG by illuminating the sample with the asymmetry factor of $\alpha=0.4$ with a fundamental beam at the resonant wavelength of 1070 nm, with a beam waist of 110 μ m, and a peak intensity of 0.62 GW/cm². The enhanced TH signal was then recorded by a spectrometer. This power level is significantly lower than the surface damage threshold for the As₂S₃ glass. Figure 4A shows that the peak TH signal from the metasurface is approximately 24 times greater than that from the reference (unpatterned) sample. As anticipated, the maximum resonant enhancement occurs near the ED-qBIC at 1070 nm, which aligns well with the calculated results presented in Figure 4B. The experimentally measured intensity of the generated TH and a broadened linear response in Figure

3a are likely due to nanofabrication-related nonuniformities in nanowire dimensions and periodicity.

Next, we study the power-dependent tunability of the device. The Kerr nonlinearity modifies the refractive index in response to the power intensity of the incident beam.³⁸ Specifically, we have $n = n_1 + \Delta n$, where $\Delta n = n_2 I$, n_1 and n_2 are the linear refractive index and the nonlinear coefficient of As_2S_3 , respectively, and *I* is the intensity of the incident beam. We first change the power of the FF beam intensity from 0.435 GW/cm² to 2.39 GW/cm², and the dependence of the THG power is shown in the log scale in Figure 4C. At lower FF intensities, the THG power exhibits the expected cubic dependence on the FF intensity. However, at higher powers, the dependence deviates from the cubic fit, with a tendency to saturate. This difference is likely due to the As₂S₃ nonlinear Kerr response in the As₂S₃, which triggers a redshift of the EDqBIC resonance while the incident fundamental beam wavelength remained fixed in our experiments. The shift of the ED-qBIC resonance, in turn, leads to a proportional spectral shift of the THG. Figure 4D demonstrates that increasing the intensity of the FF beam from 0.62 GW/cm² to 2.39 GW/cm² yields a 3 nm redshift of the THG. These shifts can be directly attributed to changes in the refractive index of As_2S_3 as a function of the input beam intensity, described by n = $n_1 + \Delta n$, where $\Delta n = n_2 I$. Here, n_1 represents the linear refractive index, n_2 is the nonlinear coefficient of As₂S₃, and I is the intensity of the fundamental beam.

As briefly discussed above, the incident angle of the FF dramatically affects the location of the resonance dip and the efficiency of the THG. For this reason, we also investigated the angular dependence of the THG from our metasurface device. The experimental setup is shown in Figure 5A: Light from a Ti: sapphire pulsed laser (100 fs pulse width, 1 kHz repetition rate) was sent to an optical parametric amplifier (OPA), which

generated near-infrared (NIR) pulses that were then directed to the propagation path via a beam splitter (BS). A 4f system, consisting of two achromatic lenses, was used for sample-laser alignment and image. The third harmonic (TH) signal was gathered by a second 4f system, which included a 50x infinitycorrected objective lens with an NA of 0.8 and additional achromatic lenses positioned behind the sample. The signal was then coupled to a spectrometer via a multimode fiber (400 µm core, 0.5 NA). The electrical field was polarized horizontally along the y-axis. The long side of the nanowires was aligned along the y-axis, and the sample was rotated around the y-axis. The detailed description of this nonlinenar measurement setup can be found in the ref 38. Figure 5B shows the measured THG spectra relative to the ED-qBIC excitation for different incidence angles. As we rotate the sample from 0° to 7.5° , the peak position of the TH shifts to a longer wavelength while the intensity reduces because sample rotation causes the ED-qBIC resonance to redshift according to modal dispersion (see Supporting Note 6). When the rotation angle reaches 10 degrees, the TH peak can no longer be detected in the frequency range under investigation. This result is confirmed by our nonlinear angular analysis (Figure 5C), which makes it clear that the ED-qBIC resonance shifts outside the spectral bandwidth of the input pulse laser. Therefore, little to no contribution of THG enhancement can be measured for this excitation angle.

4. CONCLUSIONS

In summary, we theoretically predicted and experimentally demonstrated a tunable TH generated in the lossy spectral range of As_2S_3 glass metasurfaces and its sensitivity with the incident angle. The phase-locking mechanism enables the THG and it may generally apply to other nonlinear material systems. The field localization resulting from the ED-qBIC resonance enhances the THG and the large Kerr nonlinearity of the As_2S_3 helps to achieve the tunability. These results may extend our ability to enhance nonlinear light-matter interactions and could be useful for applications in advanced switches, sensors, nanolasers, and other on-chip nonlinear nanophotonic devices.

ASSOCIATED CONTENT

Supporting Information

The Supporting Information is available free of charge at https://pubs.acs.org/doi/10.1021/acsanm.4c03200.

Notes 1–7: detailed fabrication procedure; refractive index of 300 nm As_2S_3 film measured by spectroscopic ellipsometer; simple analysis of reflectance in the k/ω space of the samples; simulated TH conversion efficiency for the three qBIC modes supported by the As_2S_3 metasurface; simulated transmittance spectrum considering the nanofabrication imprecation; angular dependence of the transmission spectrum for the As_2S_3 metasurface; Q-factors as a function of asymmetry based on eigenvalue analysis at normal incidence (PDF)

AUTHOR INFORMATION

Corresponding Author

Natalia Litchinitser — Department of Electrical and Computer Engineering, Duke University, Durham, North Carolina 27708, United States; orcid.org/0000-0002-3855-0927; Email: natalia.litchinitser@duke.edu

Authors

Jiannan Gao – Department of Electrical and Computer Engineering, Duke University, Durham, North Carolina 27708, United States

Maria Antonietta Vincenti — Department of Information Engineering—University of Brescia, 25123 Brescia, Italy

Jesse A. Frantz − US Naval Research Laboratory, Washington, D.C. 2037S, United States; ocid.org/0000-0001-7629-9932

Anthony Clabeau – University Research Foundation, Greenbelt, Maryland 20770, United States

Xingdu Qiao – Department of Electrical and Systems Engineering, University of Pennsylvania, Philadelphia, Pennsylvania 19104, United States

Liang Feng — Department of Materials Science and Engineering, University of Pennsylvania, Philadelphia, Pennsylvania 19104, United States

Michael Scalora — Aviation and Missile Center, US Army CCDC, Redstone Arsenal, Alabama 35898-5000, United States

Complete contact information is available at: https://pubs.acs.org/10.1021/acsanm.4c03200

Author Contributions

J.G., N.L., M.S., and M.A.V. developed the idea for this study. M.A.V., M.S., and J.G. performed theoretical and numerical studies. N.L. and J.G. designed and performed experiments. J.F., A.C., and J.G. deposited and characterized chalcogenide thin films. J.G., X.Q., and L.F. performed nanofabrication of the samples. All authors contributed to writing the manuscript.

Notes

The authors declare no competing financial interest.

ACKNOWLEDGMENTS

This work was supported by Office of Naval Research (ONR) awards N00014-19-1-2163 and N0001421WX01076, the NSF ECCS-1846766, OMA-1936276, NATO Science for Peace and Security program (Grant #5984) awards.

REFERENCES

- (1) Hsu, C. W.; Zhen, B.; Lee, J.; Chua, S.-L.; Johnson, S. G.; Joannopoulos, J. D.; Soljacic, M. Observation of trapped light within the radiation continuum. *Nature* **2013**, *499*, 188–191.
- (2) Hsu, C. W.; Zhen, B.; Stone, A. D.; Joannopoulos, J. D.; Soljačić, M. Bound states in the continuum. *Nature Reviews Materials* **2016**, 1, 16048
- (3) Bulgakov, E. N.; Maksimov, D. N. Topological Bound States in the Continuum in Arrays of Dielectric Spheres. *Phys. Rev. Lett.* **2017**, *118*, 267401.
- (4) Rybin, M. V.; Koshelev, K. L.; Sadrieva, Z. F.; Samusev, K. B.; Bogdanov, A. A.; Limonov, M. F.; Kivshar, Y. S. High-Q Supercavity Modes in Subwavelength Dielectric Resonators. *Phys. Rev. Lett.* **2017**, *119*, 243901.
- (5) Bernhardt, N.; Koshelev, K.; White, S. J.; Meng, K. W. C.; Froch, J. E.; Kim, S.; Tran, T. T.; Choi, D. Y.; Kivshar, Y.; Solntsev, A. S. Quasi-BIC Resonant Enhancement of Second-Harmonic Generation in WS2Monolayers. *Nano Lett.* **2020**, *20*, 5309–5314.
- (6) Sinev, I. S.; Koshelev, K.; Liu, Z.; Rudenko, A.; Ladutenko, K.; Shcherbakov, A.; Sadrieva, Z.; Baranov, M.; Itina, T.; Liu, J.; et al. Observation of Ultrafast Self-Action Effects in Quasi-BIC Resonant Metasurfaces. *Nano Lett.* **2021**, *21*, 8848–8855.
- (7) Carletti, L.; Koshelev, K.; De Angelis, C.; Kivshar, Y. Giant Nonlinear Response at the Nanoscale Driven by Bound States in the Continuum. *Phys. Rev. Lett.* **2018**, *121*, No. 033903.

- (8) Liu, Z.; Xu, Y.; Lin, Y.; Xiang, J.; Feng, T.; Cao, Q.; Li, J.; Lan, S.; Liu, J. High-Q Quasibound States in the Continuum for Nonlinear Metasurfaces. *Phys. Rev. Lett.* **2019**, *123*, 253901.
- (9) Hu, Z.; Bongiovanni, D.; Jukić, D.; Jajtić, E.; Xia, S.; Song, D.; Xu, J.; Morandotti, R.; Buljan, H.; Chen, Z. Nonlinear control of photonic higher-order topological bound states in the continuum. *Light Sci. Appl.* **2021**, *10*, 164.
- (10) Wang, Y.; Xie, B. Y.; Lu, Y. H.; Chang, Y. J.; Wang, H. F.; Gao, J.; Jiao, Z. Q.; Feng, Z.; Xu, X. Y.; Mei, F.; et al. Quantum superposition demonstrated higher-order topological bound states in the continuum. *Light Sci. Appl.* **2021**, *10*, 173.
- (11) Park, J. S.; Li, C.; Kim, K. H.; Tang, Y.; Murphey, C. G.; Teitsworth, T. S.; Kim, S.; Harutyunyan, H.; Cahoon, J. F. Optical Nonlinearity in Silicon Nanowires Enabled by Bound States in the Continuum. *ACS Nano* **2023**, *17*, 11729–11738.
- (12) Shi, T.; Deng, Z. L.; Geng, G.; Zeng, X.; Zeng, Y.; Hu, G.; Overvig, A.; Li, J.; Qiu, C. W.; Alù, A.; et al. Planar chiral metasurfaces with maximal and tunable chiroptical response driven by bound states in the continuum. *Nat. Commun.* **2022**, *13*, 4111.
- (13) Kang, M.; Mao, L.; Zhang, S.; Xiao, M.; Xu, H.; Chan, C. T. Merging bound states in the continuum by harnessing higher-order topological charges. *Light: Science & Applications* **2022**, *11*, 228.
- (14) Bogdanov, A. A.; Koshelev, K. L.; Kapitanova, P. V.; Rybin, M. V.; Gladyshev, S. A.; Sadrieva, Z. F.; Samusev, K. B.; Kivshar, Y. S.; Limonov, M. F. Bound states in the continuum and Fano resonances in the strong mode coupling regime. *Advanced Photonics* **2019**, *1*, No. 016001.
- (15) Koshelev, K.; Lepeshov, S.; Liu, M.; Bogdanov, A.; Kivshar, Y. Asymmetric Metasurfaces with High-Q Resonances Governed by Bound States in the Continuum. *Phys. Rev. Lett.* **2018**, *121*, 193903.
- (16) Anthur, A. P.; Zhang, H.; Paniagua-Dominguez, R.; Kalashnikov, D. A.; Ha, S. T.; Maß, T. W.; Kuznetsov, A. I.; Krivitsky, L. Continuous Wave Second Harmonic Generation Enabled by Quasi-Bound-States in the Continuum on Gallium Phosphide Metasurfaces. *Nano Lett.* **2020**, *20*, 8745–8751.
- (17) Hsiao, H. H.; Hsu, Y. C.; Liu, A. Y.; Hsieh, J. C.; Lin, Y. H. Ultrasensitive Refractive Index Sensing Based on the Quasi-Bound States in the Continuum of All-Dielectric Metasurfaces. *Advanced Optical Materials* **2022**, *10*, 2200812.
- (18) Xu, L.; Zangeneh Kamali, K.; Huang, L.; Rahmani, M.; Smirnov, A.; Camacho-Morales, R.; Ma, Y.; Zhang, G.; Woolley, M.; Neshev, D.; Miroshnichenko, A. E. Dynamic Nonlinear Image Tuning through Magnetic Dipole Quasi-BIC Ultrathin Resonators. Advanced. *Science* 2019, 6, 1802119.
- (19) Li, S.; Zhou, C.; Liu, T.; Xiao, S. Symmetry-protected bound states in the continuum supported by all-dielectric metasurfaces. *Phys. Rev. A* **2019**, *100*, No. 063803.
- (20) Koshelev, K.; Kruk, S.; Melik-Gaykazyan, E.; Choi, J. H.; Bogdanov, A.; Park, H. G.; Kivshar, Y. Subwavelength dielectric resonators for nonlinear nanophotonics. *Science* **2020**, *367*, 288–292.
- (21) Tan, T. C.; Srivastava, Y. K.; Ako, R. T.; Wang, W.; Bhaskaran, M.; Sriram, S.; Al-Naib, I.; Plum, E.; Singh, R. Active Control of Nanodielectric-Induced THz Quasi-BIC in Flexible Metasurfaces: A Platform for Modulation and Sensing. *Adv. Mater.* **2021**, *33*, 2100836.
- (22) Wang, B.; Liu, W.; Zhao, M.; Wang, J.; Zhang, Y.; Chen, A.; Guan, F.; Liu, X.; Shi, L.; Zi, J. Generating optical vortex beams by momentum-space polarization vortices centred at bound states in the continuum. *Nat. Photonics* **2020**, *14*, 623–628.
- (23) Yang, J. H.; Huang, Z. T.; Maksimov, D. N.; Pankin, P. S.; Timofeev, I. V.; Hong, K. B.; Li, H.; Chen, J. W.; Hsu, C. Y.; Liu, Y. Y.; et al. Low-Threshold Bound State in the Continuum Lasers in Hybrid Lattice Resonance Metasurfaces. *Laser & Photonics Reviews* **2021**, *15*, 2100118.
- (24) Wang, J.; Kühne, J.; Karamanos, T.; Rockstuhl, C.; Maier, S. A.; Tittl, A. All-Dielectric Crescent Metasurface Sensor Driven by Bound States in the Continuum. *Adv. Funct. Mater.* **2021**, *31*, 2104652.
- (25) Liang, Y.; Lin, H.; Lin, S.; Wu, J.; Li, W.; Meng, F.; Yang, Y.; Huang, X.; Jia, B.; Kivshar, Y. Hybrid anisotropic plasmonic

- metasurfaces with multiple resonances of focused light beams. *Nano Lett.* **2021**, 21, 8917–8923.
- (26) Zhang, X.; Liu, Y.; Han, J.; Kivshar, Y.; Song, Q. Chiral emission from resonant metasurfaces. *Science* **2022**, *377*, 1215–1218. (27) Gorkunov, M. V.; Antonov, A. A.; Kivshar, Y. S. Metasurfaces with maximum chirality empowered by bound states in the
- (28) He, J.; Chen, H.; Hu, J.; Zhou, J.; Zhang, Y.; Kovach, A.; Sideris, C.; Harrison, M. C.; Zhao, Y.; Armani, A. M. Nonlinear nanophotonic devices in the ultraviolet to visible wavelength range. *Nanophotonics* **2020**, *9*, 3781–3804.

continuum. Phys. Rev. Lett. 2020, 125, No. 093903.

- (29) Zhao, D.; Lin, Z.; Zhu, W.; Lezec, H. J.; Xu, T.; Agrawal, A.; Zhang, C.; Huang, K. Recent advances in ultraviolet nanophotonics from plasmonics and metamaterials to metasurfaces. *Nanophotonics* **2021**, *10*, 2283–2308.
- (30) Eggleton, B. J.; Luther-Davies, B.; Richardson, K. Chalcogenide photonics. *Nat. Photonics* **2011**, *5*, 141–148.
- (31) Li, L.; Lin, H.; Qiao, S.; Zou, Y.; Danto, S.; Richardson, K.; Musgraves, J. D.; Lu, N.; Hu, J. Integrated flexible chalcogenide glass photonic devices. *Nat. Photonics* **2014**, *8*, 643–649.
- (32) Yue, F.; Piccoli, R.; Shalaginov, M. Y.; Gu, T.; Richardson, K. A.; Morandotti, R.; Hu, J.; Razzari, L. Nonlinear Mid-Infrared Metasurface based on a Phase-Change Material. *Laser & Photonics Reviews* **2021**, *15*, 2000373.
- (33) Abdelraouf, O. A.; Anthur, A. P.; Dong, Z.; Liu, H.; Wang, Q.; Krivitsky, L.; Renshaw Wang, X.; Wang, Q. J.; Liu, H. Multistate Tuning of Third Harmonic Generation in Fano-Resonant Hybrid Dielectric Metasurfaces. *Adv. Funct. Mater.* **2021**, *31*, 2104627.
- (34) Cao, T.; Liu, K.; Tang, Y.; Deng, J.; Li, K.; Li, G. A high-index Ge2Sb2Te5-based Fabry—Perot cavity and its application for third-harmonic generation. *Laser & Photonics Reviews* **2019**, *13*, 1900063.
- (35) Zhu, M.; Abdollahramezani, S.; Li, C.; Fan, T.; Harutyunyan, H.; Adibi, A. Dynamically tunable second-harmonic generation using hybrid nanostructures incorporating phase-change chalcogenides. *Nanophotonics* **2022**, *11*, 2727–2735.
- (36) Carletti, L.; Gandolfi, M.; Rocco, D.; Tognazzi, A.; de Ceglia, D.; Vincenti, M. A.; De Angelis, C. Reconfigurable nonlinear response of dielectric and semiconductor metasurfaces. *Nanophotonics* **2021**, *10*, 4209–4221.
- (37) Gao, J.; Vincenti, M. A.; Frantz, J.; Clabeau, A.; Qiao, X.; Feng, L.; Scalora, M.; Litchinitser, N. M. Near-infrared to ultra-violet frequency conversion in chalcogenide metasurfaces. *Nat. Commun.* **2021**, *12*, 5833.
- (38) Gao, J.; Vincenti, M. A.; Frantz, J.; Clabeau, A.; Qiao, X.; Feng, L.; Scalora, M.; Litchinitser, N. M. All-optical tunable wavelength conversion in opaque nonlinear nanostructures. *Nanophotonics* **2022**, *11*, 4027–4035.
- (39) Vincenti, M. A.; Gao, J.; De Ceglia, D.; Frantz, J. A.; Scalora, M.; Litchinitser, N. M. Stacked chalcogenide metasurfaces for third harmonic generation in the UV range. *New J. Phys.* **2022**, *24*, No. 035005.
- (40) Bloembergen, N.; Pershan, P. S. Light Waves at the Boundary of Nonlinear Media. *Phys. Rev.* **1962**, *128*, 606–622.
- (41) Roppo, V.; Centini, M.; Sibilia, C.; Bertolotti, M.; De Ceglia, D.; Scalora, M.; Akozbek, N.; Bloemer, M. J.; Haus, J. W.; Kosareva, O. G.; Kandidov, V. P. Role of phase matching in pulsed second-harmonic generation: Walk-off and phase-locked twin pulses in negative-index media. *Phys. Rev. A* **2007**, *76*, No. 033829.
- (42) Mlejnek, M.; Wright, E.; Moloney, J.; Bloembergen, N. Second harmonic generation of femtosecond pulses at the boundary of a nonlinear dielectric. *Phys. Rev. Lett.* **1999**, *83*, 2934.
- (43) Roppo, V.; Centini, M.; de Ceglia, D.; Vicenti, M. A.; Haus, J. W.; Akozbek, N.; Bloemer, M. J.; Scalora, M. Anomalous momentum states, non-specular reflections, and negative refraction of phase-locked, second-harmonic pulses. *Metamaterials* **2008**, *2*, 135–144.
- (44) Koshelev, K.; Tang, Y.; Li, K.; Choi, D. Y.; Li, G.; Kivshar, Y. Nonlinear Metasurfaces Governed by Bound States in the Continuum. *ACS Photonics* **2019**, *6*, 1639–1644.

- (45) Yang, G.; Dev, S. U.; Allen, M. S.; Allen, J. W.; Harutyunyan, H. Optical Bound States in the Continuum Enabled by Magnetic Resonances Coupled to a Mirror. *Nano Lett.* **2022**, 22, 2001–2008.
- (46) Centini, M.; Roppo, V.; Fazio, E.; Pettazzi, F.; Sibilia, C.; Haus, J. W.; Foreman, J. V.; Akozbek, N.; Bloemer, M. J.; Scalora, M. Inhibition of linear absorption in opaque materials using phase-locked harmonic generation. *Phys. Rev. Lett.* **2008**, *101*, 113905.
- (47) Rodríguez-Suné, L.; Trull, J.; Scalora, M.; Vilaseca, R.; Cojocaru, C. Harmonic generation in the opaque region of GaAs: the role of the surface and magnetic nonlinearities. *Opt. Express* **2019**, 27, 26120–26130.
- (48) Fazio, E.; Pettazzi, F.; Centini, M.; Chauvet, M.; Belardini, A.; Alonzo, M.; Sibilia, C.; Bertolotti, M.; Scalora, M. Complete spatial and temporal locking in phase-mismatched second-harmonic generation. *Opt. Express* **2009**, *17*, 3141–3147.